Flow field and wake structure characteristics imposed by single seagrass blade surrogates

M. Taphorn*, R. Villanueva, M. Paul, J. Visscher, T. Schlurmann

Leibniz University Hanover, Ludwig-Franzius-Institute for Hydraulic, Estuarine and Coastal Engineering, Germany

* corresponding author: Nienburger Str. 4, 30167 Hannover; ph.:+49 511 762 14915; fax: +49 511 762 4002; taphorn@lufi.uni-hannover.de

Flow field and wake structure characteristics imposed by single seagrass blade surrogates

Seagrass surrogates are commonly used to mimic the behaviour of seagrasses exposed to currents and their effects on flow fields. The interaction is highly dependent on the chosen mechanic and geometric properties of the surrogates and needs to be understood in order to design artificial meadows. The interaction of single surrogates in unidirectional flow fields is studied by means of physical modelling. Surrogates made of plastic materials with different flexural rigidities, buoyancies and geometries are exposed to varying flow velocities. The instantaneous velocity fields in the vicinity and wake of the surrogates are measured by stereoscopic Particle Image Velocimetry (PIV). All employed surrogates disrupt and interact with the flow field by changing their posture. An empirical relation is derived between the flexural rigidity, buoyancy and characteristic diameter of the surrogates and the imposed differences in the attenuation ratio of flow velocities. Further, the approaching flow velocity and distance behind the surrogate influence the estimated attenuation. The vortex shedding frequency imposed by artificial seagrass is lower than frequencies determined for infinite, rigid cylindrical structures. Three main characterising properties: the modulus of elasticity, buoyancy and cross-sectional dimensions need to be taken into account for design of artificial seagrass meadows. Our findings advance knowledge of fluid-structure interactions of flexible materials and help to progress proper design of artificial seagrass meadows.

Keywords: artificial seagrass, submerged vegetation, stereoscopic PIV, flow-vegetation interaction, flexible surrogates

1   Introduction

Seagrass meadows in coastal environments are known to provide important ecosystem services such as dissipating energy from waves and currents, stabilising sediments and providing habitats for other marine species (Koch et al. 2006; de Boer 2007; Barbier et al. 2011; Kirkman 2014). Thus, as ecosystem engineers, seagrass meadows play an important ecological role and are considered as soft contributions to coastal protection efforts (Ondiviela et al. 2014; Spalding et al. 2014). The seagrass species *Zostera marina*

occurs in tropic, temperate, cold and polar regions on all continents of the Northern hemisphere and is thus one of the most wide-ranging seagrass species (Kirkman 2014). It is able to live in water depths of up to 50 m as well as in a wide range of temperature and short-term salinity fluctuations. Furthermore, *Zostera marina* can be found in regions with mean current velocities between 0.03 and 1.8 m/s and maximum wave heights up to 2 m (Koch 2001; Kirkman 2014).

In previous laboratory studies, living seagrass meadows (Gambi et al. 1990) as well as artificial surrogates were used to determine general effects of seagrass meadows on flow and waves. The most common material used to mimic seagrass or seaweed are plastic stripes custom-made of Polyethylene (PE) (Ghisalberti and Nepf 2002; Vettori and Nikora 2018), Polypropylene (PP) (Fonseca and Koehl 2006) or commercial plastic products such as overhead foils (Okamoto et al. 2016), cable ties and stripes of plastic folders (Bouma et al. 2005) and poly ribbon (Paul et al. 2012) were used. In some studies the blades of seagrass were represented by flexible plastic materials, while the shoots were represented by stiffer materials such as wood (Ghisalberti and Nepf 2002) or fluor elastomer (Paul and Henry 2014). In this study, artificial blades consisting of different plastic materials were used to mimic aquatic vegetation. The plant morphology was simplified in order to determine general effects of varying material properties without interaction of combined materials or interaction of blades with each other. Thus, a single blade made of homogeneous plastic material, with constant properties along its blade length, was chosen to explore the individual performance and effects imposed by single, flexible surrogates and to advance knowledge of the imposed flow field disturbances in the flexible structure's wake. As it is known from previous studies, *Zostera marina* blades have a modulus of elasticity of approximately 0.5-300 N/mm² (Patterson et al. 2001; Ghisalberti and Nepf 2002), the surrogate materials within this study were chosen accordingly. Further, the importance of buoyancy was described (Luhar and Nepf 2011; Paul and Henry 2014) in order to mimic the motion and ensure reconfiguration. The density of *Zostera marina* blades was estimated to be 0.7-0.9 g/cm³ by Luhar and Nepf (2011). While the length of the blades typically range from 30-60 cm up to 150 cm and the width from 2-10 mm (Larkum et al. 2006; Ondiviela et al. 2014), the thickness of *Zostera marina* blades ranges from 0.3-0.6 mm (Paul and los Santos 2019).

Particle Image Velocimetry (PIV) allows the simultaneous measurement of flow components in three dimensions within a plane to obtain data on the spatial distribution

of vortices and flow related fluctuations. It has been applied to investigate the effects of rigid cylindrical structures on the flow (Park and Lee 2004; Pattenden et al. 2005; Ozgoren 2006), but it has been rarely used to study the effects of flexible structures on the flow e.g. in the context of plant surrogates (Okamoto et al. 2016) or (freshwater) plants (Biggs et al. 2019). The free end of a cylinder as well as its cross-sectional shape and aspect ratio, do have an influence on the flow field, wake structure and vortex shedding (Sumer and Fredsøe 2006; Sumner 2013). While so-called tip vortices are formed at the free end that disturb and alter the local velocity field by introduction of additional turbulence, base vortices and a horseshoe vortex are formed at the bottom and probably interacting with the mobile seabed. For short cylinders, characterised by their low aspect ratio, the three-dimensional flow suppresses the formation of the vortex street or a symmetrical vortex shedding occurs (Sumner 2013). The generated vortex system around rigid cylinders has already been examined in numerous studies, however, the effects of flexible structures on the wake structure are not yet understood.

The overarching objective of this study is therefore to investigate how and to what degree single surrogates with different geometries and material properties affect the flow field and wake structure with the aim to better understand small scale turbulence within *Zostera marina* meadows which build the foundation for ecosystem services relevant for coastal protection. Hence, a flume study is conducted with measurements and analysis of the flow velocity applying the well-established PIV methodology (Adrian and Westerweel 2011). The experimental setup and details regarding the employed materials are introduced in Section 2, the results of the subsequent data analysis is presented in Section 3. Here, the main foci are set on 1) the streamwise flow velocity and its attenuation due to the presence and motion of single surrogates with varying flexural rigidity and 2) the vortex generation and changed shedding frequency due to varying material properties, cross-sectional shape and dimensions. The relation between a dimensionless parameter including the flexural rigidity, buoyancy and characteristic diameter of the surrogates and obtained flow attenuation provided by the single surrogates is summarized in an empirical derived equation. The results of this experimental study are discussed in Section 4 and in Section 5, the conclusions are presented.

2   Materials and methods

2.1   *Experimental setup*

In order to investigate the impact on the flow field and wake structure by the presence of a single artificial seagrass blade, laboratory experiments were carried out in a racetrack flume at the research facilities of the Ludwig-Franzius-Institute in Hanover.

The flume had a length of 60 m, a width of 1 m and a maximum flow depth of 0.8 m. The four installed pumps, with a total capacity of 16 kW, were able to generate flow velocities of up to 0.8 m/s in both directions (Goseberg et al. 2013; Schendel et al. 2018). During this study, a water depth of 0.4 m and unidirectional flow conditions with velocities in five steps from 0.014 m/s to 0.3 m/s were used. Within the test section of approximately 3 m length, the flume walls were made of glass, thus allowing observations and optical measurements from the side. The experimental setup of this study was placed at the downstream end of the glass walls, resulting in a distance of approximately 10 m downstream of the racetrack flumes curve and subsequent flow straightener. Further, the surrogates were positioned at a distance of 0.45 m from the outer wall of the flume.

For the hydraulic experiments, each of the six surrogates (see Section 2.2) was attached through an orifice of matching size and shape in a 4 mm-thick PVC-plate. Each surrogate was fixed from underneath, either with a short screw or with tape, to avoid any obstacles for the flow. In order to keep the plate on the ground, rails on both sides of the flume were used. The position of the plate along the x-axis was ensured through two heavy but flat mass blocks placed behind its rear edge. In this way, the exchange of surrogates was easy to manage and the position of the surrogates could be easily adjusted so that they were in the middle of the PIV's light sheet. Further, the base plate was varnished in black paint with added rhodamine B, a fluorescent dye. The rhodamine B absorbed the green light from the laser and thus reduced the reflections from the base plate. The glass of the flume was partly covered with an orange coloured adhesive foil to reduce reflections from the glass surface.

Reference experiments without surrogates were used as comparison and to confirm the unidirectional flow within the test section of the racetrack flume. These measurements showed that the standard deviation of the transversal and vertical flow components (v, w) were about an order of magnitude smaller than in the main flow direction (u). Consequently, the flow was considered to be unidirectional.
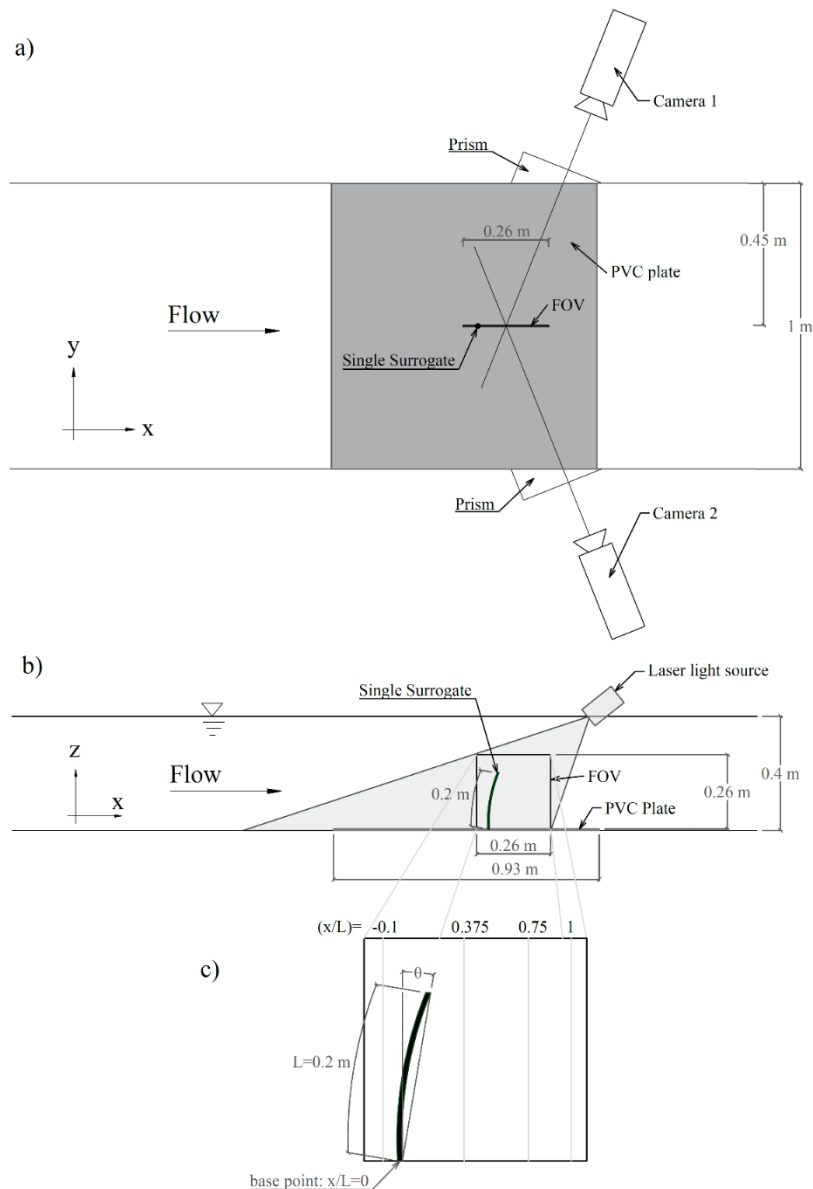
Figure 1: Experimental setup with PIV-system in (a) top view and (b) side view with an insert (c) for location of the extracted velocity profiles and angle of inclination. The flow is directed from left to right in the positive x-direction. The y-axis indicates the cross-flume direction and the z-axis is directed from the flume bottom upwards, thus indicating the water depth. The origin of the coordinate system is located at the base point of the single surrogate.

To measure the flow velocities around one single surrogate a stereoscopic PIV was employed. Two CCD-cameras (Imager ProSX 5M) with a resolution of 5 megapixels were positioned on the opposing sides of the flume with an angle of approximately 30° to the flume (Figure 1). Two water-filled prisms allowed the perpendicular alignment of the cameras to the glass walls. Pictures could thus be taken within the field of view (FOV) without image distortion caused by refraction. The cameras were calibrated to the FOV

by using a two-plane calibration plate from LaVision with dots of defined size and distance to each other. The FOV was illuminated by a double-pulsed Nd:YAG-Laser transformed to a thin light sheet. Each measurement consisted of 500 pictures (double frame) taken at a frame rate of 7 Hz. For the measurement and processing of the obtained data, the software Davis from LaVision was used. The processing was carried out using multipass stereo cross-correlation with decreasing sizes of the interrogation windows (128-32 pixel) leading to a final vector spacing grid of 1.69 mm and thus a spatial resolution of 0.35 vectors/mm². Further, tracer particles consisting of a polyamide-12-powder with a density of 1.06 g/cm³ and a diameter of approximately 50 μm were added to the fluid in order to achieve a homogeneous seeding and make the fluid motion visible and measurable through the particle displacement.

2.2 Materials

The surrogates chosen and employed in the physical experiments consisted of different plastic materials, each with a length of 20 cm. The length was thus at the lower limit of *Zostera marina* plants (Patterson et al. 2001; Paul and los Santos 2019) but allowed measurements of flow velocity fields from the flume bottom to just above the surrogates' tip. During this study, the material itself and thus the properties and cross-sectional-dimensions of the surrogates were wide-ranging (Table 1). In addition to values for the modulus of elasticity from literature, results from 3-point-bending and tensile strength tests for the individual surrogates were used. Modulus of elasticity from these measurements and the literature yielded different values for flexural rigidity of the surrogates, yet their descending order according to their flexural rigidity in table 1 remained the same.

In case of hollow surrogates made of flexible materials with a higher density than water (i.e. specimens C and E), the top and lower end were closed using hot glue. These surrogates thus contained air during the hydraulic experiments and were made positively buoyant in order to enable reconfiguration. Specimens A and D had a higher density than water as well, but due to their rigidity they either kept an upright posture even under high flow velocities (specimen A) or were able to get back to an erect position under decreasing flow velocities (specimen D).

Spec.	Material	ρ [g/cm³]	Shape of Cross section	d_i/d_o; t*w [mm]	I [mm⁴]	E_{lit} [N/mm²]	E_{meas} [N/mm²]	EI_{calc} [Nmm²]	EI_{meas} [Nmm²]	f_n [Hz]
A	Polyvinyl chloride	1.38-1.55[a]	■	4*4	21.3	1000-3500[a]	3310-3380	21300-74550	70503-71994	13.55
B	Polyethylene	0.92-0.95[a]	◉	3/5	26.7	200-1400[a]	78.8-99	5340-37380	2104-2659.3	10.27
C	Silicone	1-1.5[a] (0.64-0.96)	◎	5/8.3	202.3	8-9[b]	4.65-6.16	1618.4-1820.7	940.7-1246.2	1.77
D	Polyamide	1.13[a]	▬	1.36*4.8	1	1200[a]	658-1020	1200	658-1020	2.56
E	Silicone	1-1.5[a] (0.75-1.12)	◉	2/4	11.8	8-9[b]	2.17-2.21	94.4-106.2	25.6-26.1	0.74
F	Polypropylene	0.9[a]	—	0.11*4.8	0.0005	1100-1300[a]	149	0.55-0.65	0.075	0.065
Z. marina		0.7-0.9[e]	—	(0.3-0.6)[d]*(2-10)[e]	0.0045-0.18	0.5-300[f]		0.00225-54	0.35-3.77[d]	0.46

Table 1: Properties of the used surrogates: material and its modulus of elasticity (E) and specific density (ρ), cross-sectional dimensions (inner and outer diameter d_i, d_o, width w and thickness t respectively) and cross-sectional shape (in principal), resulting calculated second moment of area (I). Values for density (resulting density due to air-filled surrogates) and modulus of elasticity from [a] Dominighaus (2012) and [b] Henry (2014). The resulting flexural rigidities (EI_{calc}, EI_{meas}) were calculated based on modulus of elasticity available in literature and from measurements in tensile and bending tests (E_{meas}), respectively. Surrogates were sorted in descending order of their flexural rigidity. Natural frequency f_n calculated according to Equation (5). Values for Zostera marina from [c] Luhar and Nepf (2011), [d] Paul and los Santos (2019), [e] Larkum et al. (2006) and Ondiviela et al. (2014), [f] Patterson et al. (2001) and Ghisalberti and Nepf (2002)

2.3 Data analysis

For robust estimation of the flow attenuation provided by the six individual surrogates, the attenuation ratio was derived. Based on the mean streamwise velocity component (u), mean velocity profiles at various distances in the vicinity of the specimen's base point (x/L=[-0.1, 0.375, 0.75, 1]) were determined (Figure 1c). Velocity profiles were analysed and the area between each of the velocity profiles with the vertical axis (A_{vp}) was approximated by trapezoidal numerical integration (Equation 1). To determine an attenuation ratio (AtR), the area enclosed by a velocity profile in presence of a surrogate was subtracted from the area enclosed by the corresponding reference profile and subsequently related to the latter (Equation 2):

$$A_{vp} = \int_{z_b/L}^{1} \bar{u}(z)dz \approx \frac{1}{2}\sum_{n=1}^{N}(z_{n+1} - z_n)[\bar{u}(z_n) + \bar{u}(z_{n+1})], \qquad (1)$$

$$AtR = \frac{A_{vp,ref} - A_{vp,S}}{A_{vp,ref}}, \qquad (2)$$

with $A_{vp,ref}$ and $A_{vp,S}$ as enclosed area by reference velocity profiles and velocity profiles attenuated by presence of the surrogates, respectively. Despite careful preparation of the setup, measurements close to the bed did not yield trustworthy results for $z<z_b$. The values for z_b were estimated by a sensitivity analysis and used to exclude the near-bed flow velocity data from further analysis. The trapezoidal numerical integration over the mean streamwise velocity profile $\bar{u}(z)$ was restricted to the water depth z in between $z_b \leq z$ and z/L$\leq$1, with z_b/L=[0.17, 0.14, 0.09] for the approaching velocity of 0.1 m/s, 0.2 m/s, 0.3 m/s, respectively.

Proper Orthogonal Decomposition (POD) (Berkooz et al. 1993; Weiss 2019), consisting of two specific processes, was applied to instantaneous flow fields of the transverse flow component (v). At first, the instantaneous flow field was decomposed into orthogonal eigenvectors with corresponding eigenvalues. Secondly the most powerful eigenmodes were applied to reconstruct and approximate the instantaneous flow field. As a result, coherent flow structures became more distinct and evaluable within the approximated instantaneous flow fields.

In this study, the 25 most powerful eigenmodes were used to approximate the instantaneous flow fields. As the flow fields in this study contained a lot of small-scale turbulence, including a relatively large portion of energy, more eigenmodes than usual (Weiss 2019) were needed to approximate the flow fields with well represented vortices.

A sensitivity analysis showed that a higher number of eigenmodes led to a higher accuracy in approximation of the flow field as small-scale turbulence was represented. The shed vortices, as the striking features of the flow were not evaluable. In contrast, a lower number resulted in smoothed out shedding vortices.

The result of the POD was 500 approximated flow fields. The out-of-plane velocity component (v) was used for further analysis as the generated vortices could only be characterized in this flow velocity component. For each test case, a proper location for characteristic vortices was determined at which the flow velocity is extracted for further analysis. As the formation of structure-induced vortices appeared to evolve properly in a certain distance downstream of the surrogate, the location was chosen in close vicinity to the surrogate in x-direction but depended on the specimen and its inclination. The z-coordinate was selected around ¾ of the affected flow height as the vortices were more distinct with increasing distance from the flume bottom but were influenced close to the surrogates' tip by the flow above. The extracted time series of flow velocity (v), containing oscillations due to the vortices, was analysed by using a Fast Fourier Transformation (FFT). With this method the main frequencies of the structure-induced shed vortices were determined. Within the results, the dimensionless Strouhal number (Equation 3) was used to assess the normalized shedding frequencies for all surrogates to compare the different geometries. The Strouhal number is defined as the vortex shedding frequency f_v normalized by the cylinder diameter D and the flow velocity U (Sumer and Fredsøe 2006):

$$St = \frac{f_v D}{U}. \tag{3}$$

The wake structure was also dependent on the flow properties. Therefore the Reynolds number, representing the ratio of inertial forces to viscous forces was calculated according to Equation 4. The Reynolds number is used to classify the flow structure without dimensions:

$$Re = \frac{UD}{v}, \tag{4}$$

where D is the diameter of the cylinder, U is the flow velocity and v is the kinematic viscosity of the fluid (Sumer and Fredsøe 2006). The natural frequencies of the surrogates were determined according to Equation 5 in order to examine if the condition for resonance needs to be taken into account:

$$f_n = \frac{a_i}{2\pi} \sqrt{\frac{EI}{(\mu+A')L^4}}, \tag{5}$$

where EI is the flexural rigidity, L is the length and μ is the mass per unit length of the surrogates. Further, $a_1=3.52$ is the numerical constant for a cantilever beam in first vibration mode and $A'=K\rho\pi c^2$ is the added mass of the submerged surrogates. Herein, c is half the diameter or half the width of the specimen and K is either 1 (circular and slender rectangular cross sections) or 1.51 for specimen A with square cross section (Naudascher and Rockwell 1994). The flexural rigidity EI is the product of the modulus of elasticity E and the second moment of area I. The latter was calculated dependent on the cross-sectional shape of the specimen, for rectangular cross sections:

$$I_{rect.} = \frac{wt^3}{12}, \tag{6}$$

and for annular cross-sections:

$$I_{ann.} = \frac{\pi}{64}\left(d_o{}^4 - d_i{}^4\right), \tag{7}$$

with the cross-sectional dimensions inner (d_i) and outer diameter (d_o), width w and thickness t of the specimen.

3   Results

All surrogates responded to the approaching flow by bending along the flume's x-axis. In all cases except for surrogate A, increasing flow velocities led to increased inclination. The presence of an artificial single blade had a measurable effect on the flow field. The damping effect differed in magnitude and extent depending on the surrogate's material properties, cross-sectional shape and dimensions as well as the magnitude of the approaching flow velocity. This damping effect was only observed in the mean streamwise velocity component (u). However, an effect on the instantaneous flow field was also detected in the stream normal component (v) as vortices shed and propagate downstream within the wake of the surrogates.

3.1   Flow attenuation

In general, the damping effect by single blade surrogates was apparent in reduced flow velocities in its wake. This was especially the case close to the surrogate (Figure 2)

where velocities at the same vertical (*z*) position were higher in front of the surrogates than in their wake. This effect decreased with increasing downstream distance from the surrogate. Further, the attenuation decreased in magnitude with increasing flow velocities. Due to an enhanced bending of the flexible structures with flow velocity (Figure 3), the area of reduced flow velocities in the wake of the surrogates was decreased in size and changed in shape (Figure 2). Therefore the velocity profiles were influenced by the reconfiguration of the surrogates as an attenuation of flow velocity only occurred up to the bent height of each flexible surrogate (Figure 4). The measured velocity profiles upstream of the surrogates aligned in shape with the reference profiles but the velocity magnitude differed between the reference case and the experiments with different surrogates. This indicates that the surrogates also affect the flow upstream, at least up to the distance of x/L=-0.1 from the specimen (Figure 4).
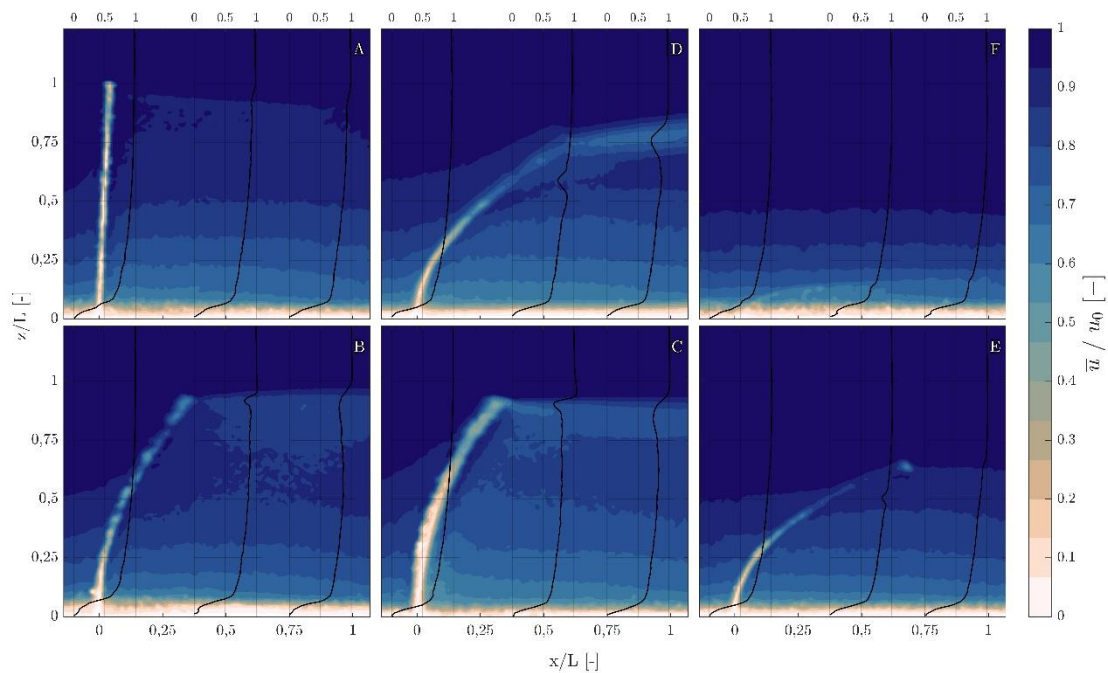

Figure 2: Mean streamwise flow velocity component (u) in the FOV related to approaching flow velocity u_0=0.3 m/s (average over flow depth). Background colours dependent on dimensionless flow velocity. Each subplot depicts one individual experiment with one of the six surrogates (see Section 2) with the top row containing the specimens with square or rectangular cross-sections (A, D, F) and the bottom row containing the specimens with annulus cross-sections (B, C, E).

Values used for the overlaid velocity profiles are extracted from the 2-dimensional mean streamwise velocity field along three vertical lines at distinct distances along the x-axis from the surrogate's base point (-0.1 x/L, 0.375 x/L, 0.75 x/L). The corresponding axis including the zero-line at which the velocity values are extracted, is displayed in light grey.

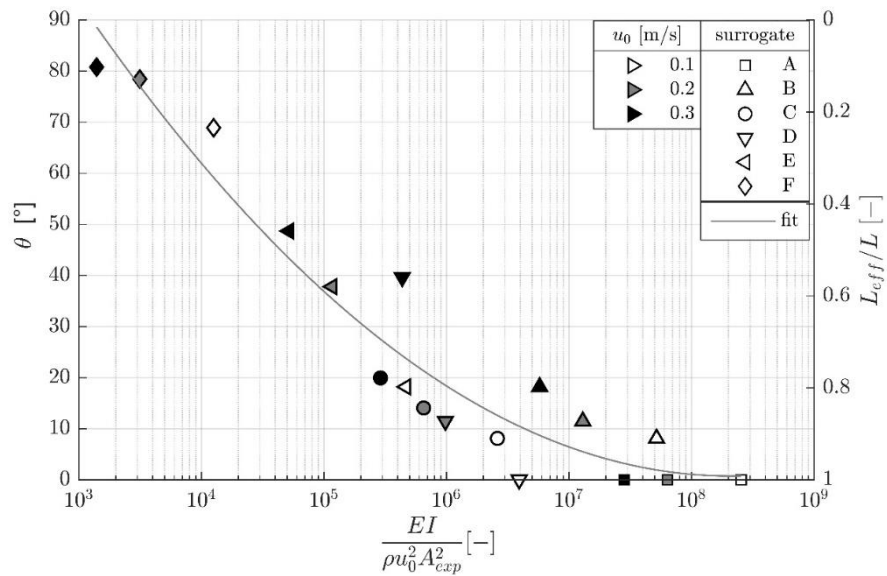*Figure 3: Inclination angle θ [°] and relative effective length L_{eff}/L of the surrogates A-F related to their flexural rigidity EI divided by density ρ, approaching flow velocity u_0 and exposed area A_{exp}. The marker type indicates the surrogate and their filling depends on the approaching flow velocity u_0 (unfilled: 0.1 m/s, filled grey: 0.2 m/s, filled black 0.3 m/s).*

Apart from the general properties, the attenuation behaviour could be categorised based on the results. The first characteristic attenuation effect is represented by specimen A with the highest flexural rigidity and no change in posture. The velocity profiles had the same shape regardless of the approaching flow conditions and distance behind the surrogate itself. The attenuation ratio (AtR) varied between 5 and 9 % for positive x/L-values (Figure 5). Only small discrepancies occurred for each location and flow velocity in the wake with a maximum difference of 2 % respectively and thus remains relatively constant. On the other hand, the two surrogates with the lowest flexural rigidity (E and F) affected the velocity profiles either in a weaker manner or up to comparable attenuation values than specimen A (i.e. for specimen E, u_0=0.1 m/s, see Figure 4 and Figure 5). Further, the shape of the affected velocity profiles is comparable between these three specimens (Figure 4).
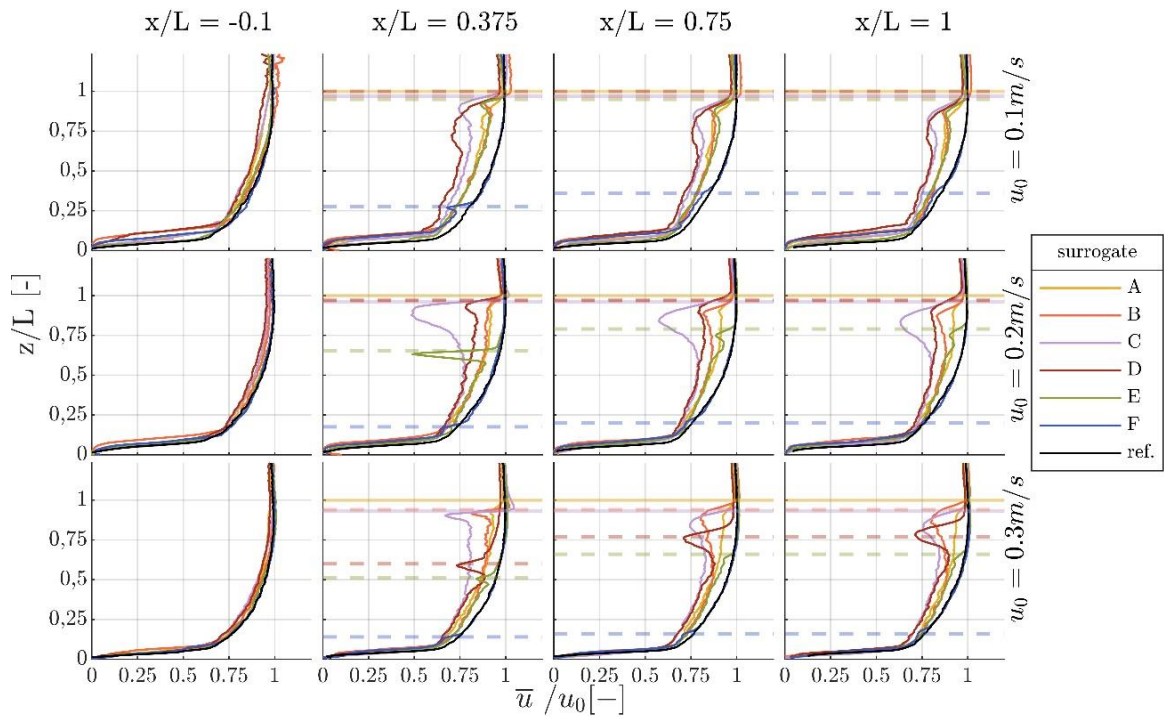
Figure 4: Mean streamwise velocity profiles related to approaching flow velocity. Six velocity profiles in different colours according to the employed surrogates (A-F) and a reference velocity profile (black), generated in experiments without any surrogate are displayed for each x-location and flow velocity. The location along the x-axis differs column wise (x/L=-0.1, x/L=0.375, x/L=0.75, x/L=1) and the three approaching velocities (0.1 m/s, 0.2 m/s and 0.3 m/s) are applied row wise. Horizontal (dashed) lines indicate either the position of the corresponding surrogates tip or the maximum height reached at the corresponding location.
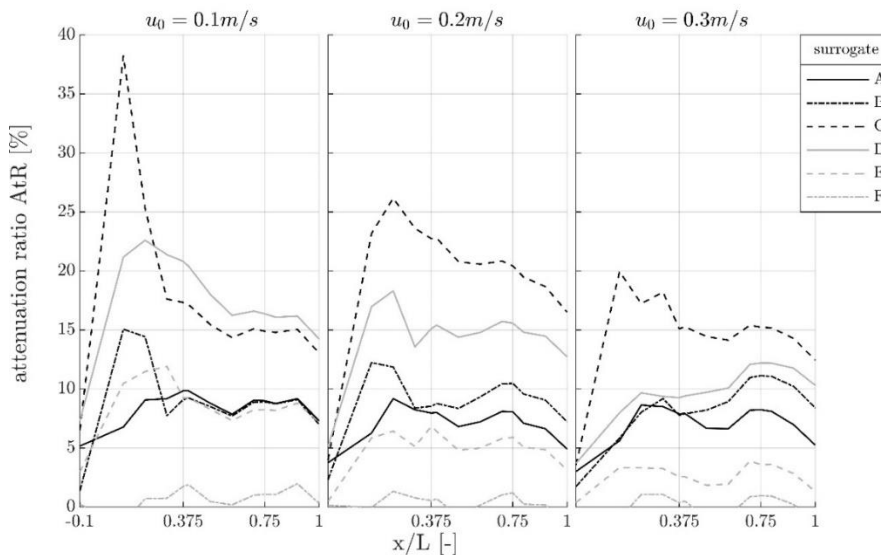

Figure 5: Attenuation ratio dependent on the distance along the x-axis from the surrogate's base point. The approaching flow velocity differs column wise (0.1 m/s, 0.2 m/s, 0.3 m/s), the six employed surrogates are represented by varying line styles and colour.

The remaining surrogates (B, C, D) had intermediate flexural rigidities and were leading to overall higher flow attenuation ratios (7 to 38 %). Among these surrogates, the velocity profiles were affected to the greatest extent and the shape deviates strongly from the reference profile. A local minimum in flow velocity, i.e. maximum in flow attenuation could be observed just below the tip which was either caused by the generated tip vortices or by the surrogates themselves (see section 3.2).

Moreover, for surrogates with a relatively low flexural rigidity, i.e. specimen D, E and F ($EI \leq 1200$ Nmm²) the ability to attenuate the flow decreased with rising velocities. In contrast, specimens B and C showed diverging trends in attenuation, dependent on flow velocity and distance. The attenuation provided by specimen C was the highest for each of the flow conditions except for u=0.1 m/s when x/L>0.3. This inhibits also the overall maximum in flow attenuation. When excluding the peak at u=0.1 m/s, x/L=0.1, the highest deceleration in presence of specimen C was obtained at medium flow velocities. For specimen B, the attenuating effect decreased close to the surrogate and increased downstream (x/L=0.75) with flow velocity. This relocation of the maximum attenuation in downstream direction with increasing flow velocity was also obtained for specimens D and E (Figure 5).

As specimens C and E consisted of the same material and both had a hollow circle in cross-sectional shape, the differences in their attenuation behaviour was only caused by their diameter ($d_C > 2 \cdot d_E$) resulting in different values for flexural rigidity. Specimen C had a stronger effect on the flow with attenuation ratios between 12.5 and 38.2 % (behind the surrogate) than specimen E with ratios from 1.3 to 11.9 %. This suggests a non-linear effect of the diameter on flow attenuation due to a larger flow-obstructing structural area and a higher second moment of area resulting in a higher structural rigidity.

Overall, the attenuation ratio depends mainly on the flexural rigidity (EI). To a lesser extent, the approaching flow velocity and the distance behind the surrogate also affects the attenuation (Figure 6). The attenuation ratio can be roughly approximated by a 5th order polynomial equation (Equation 8):

$$AtR = 0.142\,X^5 - 0.577\,X^4 - 1.069\,X^3 + 3.303\,X^2 + 6.042\,X + 2.284 \ , (8)$$

where the dimensionless variable X is:

$$X = \log\left(\frac{EI}{\rho u_0{}^2 A_{exp} x D_{ch}}\right) , \qquad (9)$$

derived from dimensional analysis with the flexural rigidity EI, material density
ρ, approaching flow velocity u_0, distance behind the surrogates base x and characteristic
diameter D_{ch}. The latter is either the width of the specimen (circular or square cross sec-
tion) or the outer diameter. The projected area exposed to the flow $A_{exp}=D_{ch}L_{eff}$ was cal-
culated with the characteristic diameter and effective length L_{eff} , the perpendicular dis-
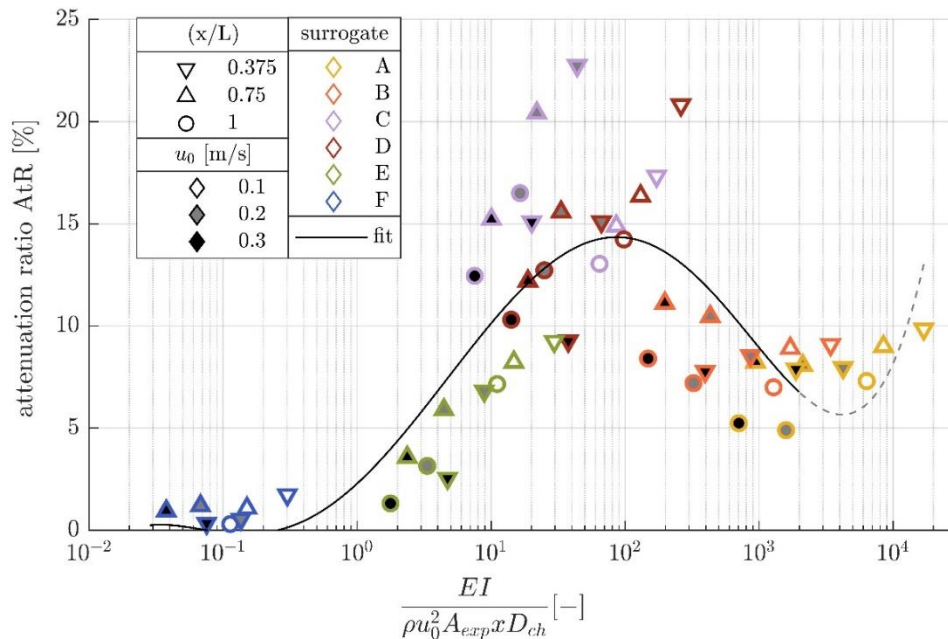tance between the flume bottom and the surrogates mean tip position.

Figure 6: Attenuation ratio (AtR) dependent on flexural rigidity (EI) and density ρ as material properties of the surro-
gates A-F (edge colour), further dependent on flow velocity u_0 (filling colour) and distance behind the surrogate x/L
(marker type). A_{exp} is the projected area exposed to flow and D_{ch} represents the characteristic diameter, e.g. the outer
diameter or width of the surrogates. The upturn of the fitted curve for X>3*10^3 is expected to be an overestimation
for the data and a mathematical artefact. Therefore, this part is presented with a dashed line.

3.2   Tip vortices

The mean flow velocities indicated also the presence of tip or trailing vortices for
some of the specimens under certain flow conditions. These tip vortices caused by the
free end of the surrogates became apparent through locally reduced flow velocities down-
stream of the surrogate's tip in the flow field and extracted velocity profiles (Figure 2
andFigure 4).

For the approaching flow velocity of 0.3 m/s (Figure 2), the tip vortices became
visible for specimens C and D and in a weaker manner for specimen B, as the inclination
of the surrogates strengthened the vortices if the inclination and motion remained within
a certain range. For this flow condition, the tip vortices were not apparent in the wake of

specimen E and F as their tip position is too low and their tip motion too high. The tip vortices became weakly apparent for the approaching velocity of 0.1 m/s also in the wake of specimen E when its inclination was comparable to the inclination of specimen C at 0.3 m/s (Figure 3).

While the tip vortices could be distinguished and characterised by local minima in flow velocity profiles, they should not be confused with the distinct, sharply defined peaks caused by the presence of the bent surrogates itself. The latter occurred if the surrogates are bent strong enough to intersect with the first axis of extracted velocity profiles (x/L=0.375) dependent on the material properties and flow velocity and could only be observed in some of the test cases (e.g. F for 0.1 m/s, E for 0.2 m/s and C, D, E for 0.3 m/s).

3.3   Vortex generation

In addition to effects on the mean flow field, the surrogates led to vortex shedding and thus also affected the instantaneous flow field, becoming evident in the transverse flow component (v). Within the experiments, the Reynolds number varied between 56.8 and 2490. Therefore the wake regime had an appearance of a vortex street which could be categorized into laminar vortex street ($40 < Re < 200$), transition state to turbulence in the wake ($200 < Re < 300$) up to completely turbulent wakes ($300 < Re < 3*10^5$) (Sumer and Fredsøe 2006). Due to the low sampling rate of the PIV-system (7 Hz) an evaluation of shedding frequencies was only possible for all specimen at low velocities and specimen C with larger diameter at higher velocities.

First, Proper Orthogonal Decomposition was applied to the flow fields as described in Section 2.3 leading to flow fields with clearly observable and evaluable shedding vortices as expected for this flow regime (Figure 7). In general, the shed vortices moved faster downstream with increasing flow velocity. Due to slightly different flow velocities along the surrogate's axis, the velocity of the vortices' downstream propagation was higher with increasing distance from the flume bottom and thus the shed vortices were inclined. As a result, the regular structure of vortices was broken up occasionally and a reconnection to other vortices took place within the area lower than half the bent surrogate. Further, the inclination of the surrogates was not equal to the inclination of vortices in the wake (e.g. Figure 7).
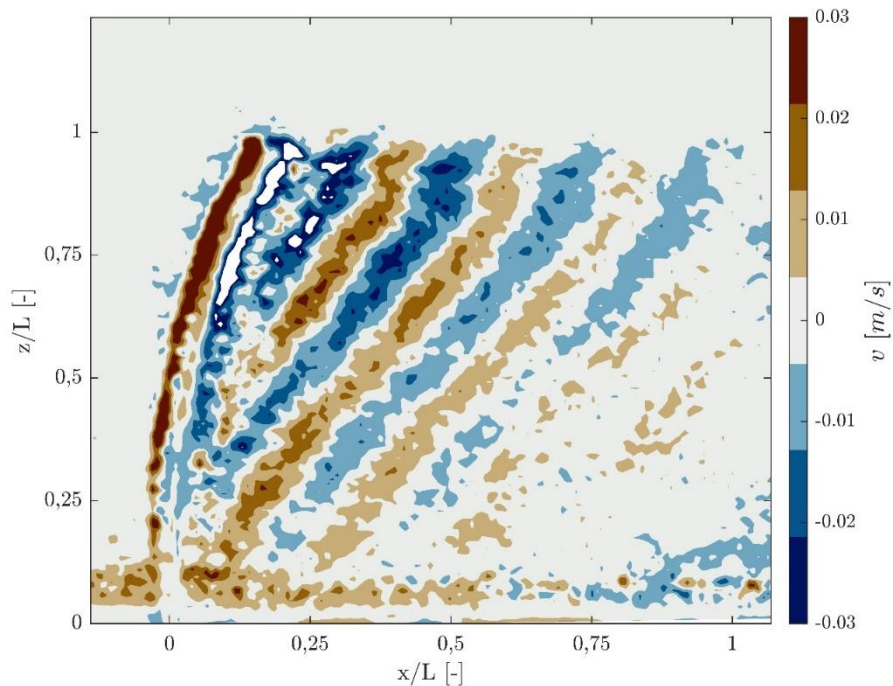
Figure 7: POD result showing the approximated instantaneous transverse velocity component (v) within the FOV. As an example, the result for an approaching velocity u_0=0.1 m/s in presence of surrogate C is shown. Red and blue coloured areas representing positive and negative values for the velocity component, respectively.

The resulting vortex shedding frequencies from the FFT based on the POD results were normalized using the corresponding outer diameter or width of the surrogate and the approaching flow velocity in accordance to Equation 3. The normalized vortex shedding frequency, in relation to the Reynolds number (Figure 8), was lower for the surrogates than for idealized two dimensional and rigid cylinders with circular or rectangular cross sectional shape, respectively (Roshko 1954; Fey et al. 1998; Sumer and Fredsøe 2006). As in this study the surrogates were finite and fully submerged structures, the flow around the single blade surrogates was affected three dimensionally by their free end. The flow above the surrogates remained unidirectional and undisturbed, thus having higher stream-wise velocities than in the wake, leading to a shear flow. The latter affected the flow in the wake resulting in lower shedding frequencies as observed by Park and Lee (2004). For cylinders with a low aspect ratio (AR<7.5) the vortex shedding could even be suppressed due to the free end (Park and Lee 2004).

Furthermore, the flexural rigidity of the surrogates had an effect on the wake structure. As the surrogates were only fixed at one base point and made of flexible materials, they bent and moved due to the approaching flow and the resulting vortex shedding. Their

inclination led to lower shedding frequencies as the vortex generation took place at a
slightly varying location along the x-axis, dependent on the surrogates bending behaviour
and thus their flexural rigidity. As a result, the vortex generation was initialized the ear-
liest within the area close to the base, as it was the most upstream location of the bent
suurogate. Due to a slightly lower flow velocity the shedding frequency was also lower
here. This affected the further vortex generation along the surrogates axis to a slightly
reduced vortex shedding frequency overall, as was also observed by Vlachos and Telionis
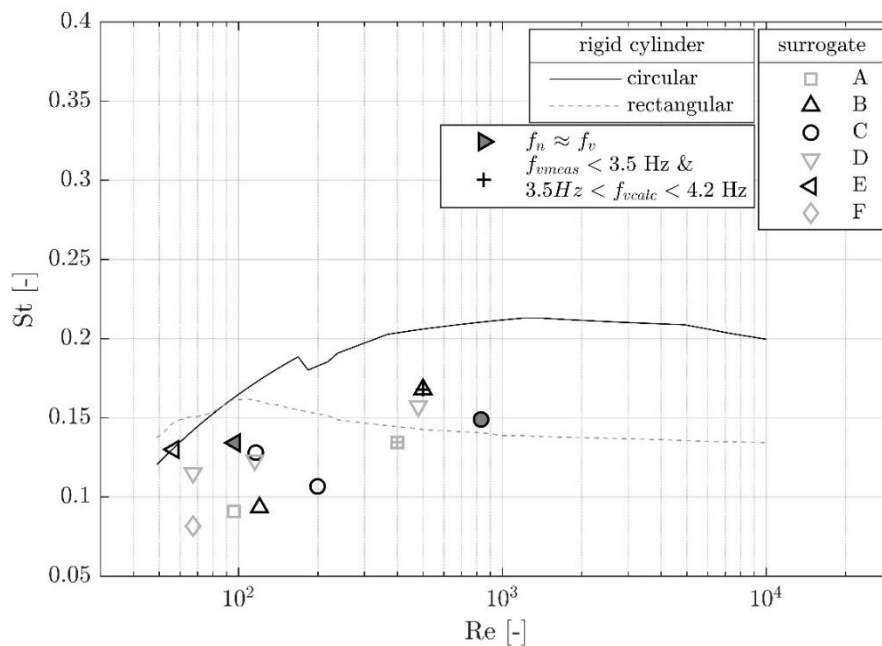(2008) for inclined emergent cylinders.

*Figure 8: Vortex shedding characterized by dimensionless vortex shedding frequency (Strouhal number) and Reynolds
number in comparison to values determined for infinite cylinder with circular (black line) and rectangular cross-sec-
tional shape (dotted light grey line) from (Sumer and Fredsøe 2006), Roshko (1954), Fey et al. (1998). Data points
marked according to the six surrogates, black markers used for specimen with circular cross-sectional shape (B, C, E)
and light grey for square and rectangular cross-sectional shape (A, D, F), respectively. Filled markers indicate cases
where the vortex shedding frequency is approximately equal to natural frequency, crossed markers indicate cases
where the measured shedding frequency is lower than 3.5 Hz while the calculated frequency is slightly above.*

Additionally, the vortex shedding caused the flexible surrogates to move. This
motion of the surrogates, in turn could have interacted with the vortex shedding and thus
affected the frequency of this process. Vortex shedding results in a force acting on the
surrogates and could be the reason for transverse motions of the flexible specimens. As
the vortex shedding is tied to the structure causing the process, it still occurred behind the
new position of the surrogate which could lead to a deceleration of the shedding process

by the motion. As a result, the vortex shedding frequency was diminished due to the motions of the flexible surrogates, confirming the results from Jung et al. (2018).

For most of the analysed test cases, the vortex shedding frequencies were significantly higher or lower than the natural frequency of the specimen. However, in two cases the estimated vortex shedding frequency is approximately the same as the natural frequency, e.g. specimen C with u_0=0.1 m/s and specimen E with u_0=0.024 m/s (Figure 8). However, the resonance effect could not be verified without reliably determined motion of the surrogates.

4   Discussion

The present study investigated how the flow field and wake structure were affected by the presence of single surrogates. A dependence of the attenuation ratio on flexural rigidity, buoyancy and characteristic diameter of the individual surrogates as well as on the flow velocity and distance behind the surrogate was found.

The inclination of the surrogates increased with flow velocity, as well as their motion. The latter was not only observable in the physical model tests but was also evident in the mean streamwise velocity fields. However, the motion could not be analysed as the sampling frequency of 7 Hz did not provide sufficient temporal resolution. In the measurement period of 500 images, the motion showed high frequencies and irregularities in a mostly three-dimensional motion. The experimental setup was intended to measure flow velocities also in close vicinity of the surrogates. For this reason the specimens were painted black in order to eliminate reflections. As a result, the surrogates position could not be reliably estimated whenever it moved out of the laser light sheet. Moreover, the low pre-curvature of specimens B and C caused by production processes and storage of these tubes affected their inclination. For these surrogates, it was not possible to remove the pre-curvature completely before conducting the physical model tests. Lower inclination angles are expected if the material would have been perfectly straight, especially for low flow velocities.

The attenuation ratio caused by the surrogates differs greatly for the same material but different cross-sectional dimensions (specimens C and E). To a lesser extent the attenuation ratio differs for the same cross-sectional dimensions and shape but different material (specimens B and E). Consequently, the dimensions appear to be of greater importance for attenuation than the material properties. However, the highest attenuation

ratios can be achieved through different cross-sectional shapes (surrogate C circular, surrogate D rectangular) for intermediate, quite similar flexural rigidities. Thus the shape of the cross-section plays a smaller role than the overall flexural rigidity in terms of flow attenuation. As the flexural rigidity is composed of the product of the modulus of elasticity and the second moment of area, different combinations of material, cross-sectional dimension and shape might lead to the optimum value for flexural rigidity in terms of flow attenuation. The flow attenuation of the specimens investigated here (Figure 6) shows a certain distribution dependent on the surrogate properties and flow conditions which was roughly approximated with the polynomial fit. However, the specimens show deviations and differing characteristics which cannot be fully explained within the scope of this study. In this context, we hypothesize that the motion of the flexible surrogates might play an important role in the observed scatter of the data. However, for an analysis of the specimens' motion, the data is not of sufficient quality.

The analysis of wake structure showed that the vortex shedding frequency in the wake of all six surrogates was lower (Figure 8) than for infinite, rigid cylinders with circular or rectangular cross-sectional shape, respectively (Sumer and Fredsøe 2006). However, the sampling frequency of the PIV system does not provide optimal conditions for analysis of the vortex shedding frequencies in the wake, as the detectable frequencies are limited to a maximum of 3.5 Hz. The determined vortex shedding frequencies for the flexible surrogates of this study were below 3.5 Hz even for higher Reynolds numbers (Re>1000). In contrast, calculations of vortex shedding frequencies based on data from the literature (Sumer and Fredsøe 2006) lead to values above 3.5 Hz by use of the corresponding characteristic diameter and flow velocity of this study. Thus the cases with high discrepancies (f_{calc}>4.2 Hz) were not displayed here and the cases with slightly higher calculated vortex shedding frequencies (f_{meas} <3.5 Hz<f_{calc}<4.2 Hz) were marked with a cross (Figure 8). The natural frequency of the submerged surrogates was significantly higher or lower than the vortex shedding frequency for most of the test cases, and resonance effects were only conceivable for two of the analysed data sets. However, a resonance effect could not be verified as the motion of the surrogates in out-of-plane direction could not be reliably determined.

Even though the surrogates investigated within this study represent single blades rather than complete seagrass shoots, implications for seagrass meadows can be derived. It should be noted, however, that these implications can only be described qualitatively

at this stage, since the surrogates lack the more rigid stem seagrass shoots exhibit at the base and are located lower in the water column as blades sitting on top a stem would be. But since all the surrogates led to reduced streamwise flow velocities and generated vortices in their wakes, an influence on downstream located plants or surrogates in a meadow is implied. The reduced flow velocity leads to reduced hydrodynamic load on plants or surrogates behind. Therefore every seagrass plant provides a minimum shelter for the ones behind.

The reduced flow velocity also causes enhanced sedimentation within and behind seagrass meadows (de Boer 2007). On the other hand the wake structure might cause a suppression of sediment settling due to the locally and temporarily increased flow velocities in the vortices. Additionally, this could lead to local erosion and scour (Lefebvre et al. 2010). Furthermore, seagrass plants are known to rescale turbulence as the generated turbulence eddies (caused by the presence of the plants) are transformed into smaller eddies depending on the distance between the shoots (Koch et al. 2006). Thus the coherent vortices determined in the wake of single blade surrogates within this study are expected to be rescaled due to other shoots in the vicinity in a meadow setting, leading to smaller turbulences within a meadow. This turbulence could lead to an occasionally decreased leaf surface boundary layer causing enhanced nutrient availability to seagrass plants (Fonseca and Kenworthy 1987) and promotes the exchange of nutrients and the transport of pollen (Koch 2001).

Given that the reduced vortex shedding frequency on submerged aquatic vegetation can have positive (lower drag forces) and negative effects (reduced nutrient exchange) for the vegetation, the overall role for seagrass health and development is not yet known. However, future research should evaluate how knowledge on vortex shedding frequency can support understanding of ecological processes within seagrass meadows.

The attenuation ratio was determined for wide-ranging surrogate properties and the flexural rigidity was characterized as being of high importance. The determined relationship can be used to roughly predict the effect imposed by a single blade surrogate for a wide range of chosen material. However, the derived relationship is only valid for single blades and cannot be transferred to complex plant morphologies or meadows with interacting plants and blades. The attenuation ratio shows a maximum for surrogates of intermediate flexural rigidities ($658 < EI < 1820$ Nmm²) resulting in the highest efficiency in terms of flow reduction. *Zostera marina* has a flexural rigidity of 0.35 to 3.77 Nmm² (Paul

and los Santos 2019), which lies between the values of specimens E and F. Even with a slightly lower density of *Zostera marina* blades, it can be assumed that the relationship found for a wide range of material properties in Figure 3 is also valid for *Zostera marina* blades. Therefore the area exposed to flow will also lie between the values of specimens E and F. As a result, for a *Zostera marina* blade the achieved values for the term $EI/(\rho u_0{}^2 A_{exp} x D_{ch})$ would lie in between the values of specimens E and F for the same flow conditions. Thus, it is expected that a single blade of *Zostera marina* would lead to values of attenuation between those achieved for specimens E and F (Figure 6 and Equation 8). In effect, by using the most efficient surrogates in terms of flow attenuation the condition of resembling seagrass plants cannot be fulfilled.

5   Conclusion

A laboratory investigation was conducted to determine the effects of single surrogates on flow fields and wake structure with highly resolved PIV measurements. The surrogates were made of various plastic materials in order to estimate effects of flexural rigidity and cross-sectional dimensions on the attenuation ratio. This study demonstrated that each of the six single surrogates affected the streamwise velocity fields and extracted velocity profiles. While the streamwise velocity component was reduced up to the bent height of the specimen for surrogates with a distinct inclination, also tip vortices could be estimated. These vortices are characterized by a strongly reduced streamwise velocity behind the tip. The attenuation ratio provided by different materials showed characteristics dependent on the flexural rigidity, buoyancy, flow velocity and distance behind the surrogate, for which an empirical relation was derived. For surrogates with intermediate flexural rigidity the highest attenuation ratio was achieved. The empirical relationship was derived for wide-ranging properties of surrogates thus can be applied to predict the attenuation provided by single blades of several materials.

Furthermore, the wake structure was examined for each of the six surrogates based on normalized vortex shedding frequencies. Due to their flexural rigidity and resulting inclination under certain flow conditions as well as their free end, the vortex shedding frequency was lower than predicted by Sumer and Fredsøe (2006) for the two dimensional circular or rectangular cylinder, respectively.

For the development and design of artificial seagrass meadows it is important to consider the properties of the chosen material. The material properties and surrogates

dimensions result in differing ability to alter currents, whereby the flexural rigidity is of high importance. Further, the artificial plants should be able to reconfigure either due to their rigidity or due to their density, being positively buoyant. This study shows that the cross-sectional shape plays a minor role for flow reduction and vortex shedding frequency. The highest flow attenuation could be achieved either with a rectangular (surrogate D) or a circular cross-sectional shape (surrogate C) while the diameter here was approximately double of the width. However, in combination with the different modulus of elasticity, comparable flexural rigidities were achieved. Thus, for a proper design of artificial seagrass meadows it is recommended to account for an appropriate combination of the three main characterising material properties.

References

Adrian RJ, Westerweel J. 2011. Particle image velocimetry. Cambridge: Cambridge Univ. Press. 558 p. ISBN: 9780521440080. eng.

Barbier EB, Hacker SD, Kennedy C, Koch EW, Stier AC, Silliman BR. 2011. The value of estuarine and coastal ecosystem services. Ecological Monographs. 81:169–193. doi:10.1890/10-1510.1.

Berkooz G, Holmes P, Lumley JL. 1993. The Proper Orthogonal Decomposition in the Analysis of Turbulent Flows. Annu. Rev. Fluid Mech.:539–575.

Biggs HJ, Nikora VI, Gibbins CN, Cameron SM, Papadopoulos K, Stewart M, Fraser S, Vettori D, Savio M, O'Hare MT, et al. 2019. Flow interactions with an aquatic macrophyte: a field study using stereoscopic particle image velocimetry. Journal of Ecohydraulics. 4:113–130. doi:10.1080/24705357.2019.1606677.

Bouma TJ, Vries MBd, Low E, Peralta G, Tánczos IC, van de Koppel J, Herman PMJ. 2005. Trade-offs related to ecosystem engineering: a case study on stiffness of emerging macrophytes. Ecology. 86:2187–2199. doi:10.1890/04-1588.

de Boer WF. 2007. Seagrass–sediment interactions, positive feedbacks and critical thresholds for occurrence: a review. Hydrobiologia. 591:5–24. doi:10.1007/s10750-007-0780-9.

Domininghaus H. 2012. Kunststoffe: Eigenschaften und Anwendungen [plastic materials: properties and applications]. 8th ed. Elsner P, Eyerer P, Hirth T, editors. Berlin: Springer (VDI-Buch). ISBN: 9783642161735. german.

Fey U, König M, Eckelmann H. 1998. A new Strouhal–Reynolds-number relationship for the circular cylinder in the range 47<Re<2×105. Physics of Fluids. 10:1547–1549. doi:10.1063/1.869675.

Fonseca MS, Kenworthy W. 1987. Effects of current on photosynthesis and distribution of seagrasses. Aquatic Botany. 27:59–78. doi:10.1016/0304-3770(87)90086-6.

Fonseca MS, Koehl M. 2006. Flow in seagrass canopies: The influence of patch width. Estuarine, Coastal and Shelf Science. 67:1–9. doi:10.1016/j.ecss.2005.09.018.

Gambi MC, Nowell ARM, Jumars PA. 1990. Flume observations on flow dynamics in Zostera marina (eelgrass) beds. Marine Ecology Progress Series. 61:159–169.

Ghisalberti M, Nepf H. 2002. Mixing layers and coherent structures in vegetated aquatic flows. J. Geophys. Res. 107. doi:10.1029/2001JC000871.

Goseberg N, Wurpts A, Schlurmann T. 2013. Laboratory-scale generation of tsunami and long waves. Coastal Engineering. 79:57–74. doi:10.1016/j.coastaleng.2013.04.006.

Henry P-YT. 2014. Bending properties of a macroalga: Adaptation of Peirce's cantilever test for in situ measurements of Laminaria digitata (Laminariaceae). American Journal of Botany. 101:1050–1055. en. doi:10.3732/ajb.1400163.

Jung SY, Kim JJ, Park HW, Lee SJ. 2018. Comparison of flow structures behind rigid and flexible finite cylinders. International Journal of Mechanical Sciences. 142-143:480–490. doi:10.1016/j.ijmecsci.2018.05.026.

Kirkman H. 2014. Near-Coastal Seagrass Ecosystems. In: Monson RK, editor. Ecology and the Environment. New York, NY, s.l.: Springer New York; p. 457–482 (The Plant Sciences; vol. 8).

Koch EW. 2001. Beyond Light: Physical, Geological, and Geochemical Parameters as Possible Submersed Aquatic Vegetation Habitat Requirements. Estuaries. 24:1. doi:10.2307/1352808.

Koch EW, Ackerman JD, Verduin J, Keulen M. 2006. Fluid Dynamics in Seagrass Ecology—from Molecules to Ecosystems. In: Larkum AWD, Orth RJ, Duarte CM, editors. Seagrasses: Biology, ecology and conservation;. Dordrecht: Springer; p. 193–225.

Larkum AWD, Orth RJ, Duarte CM, editors. 2006. Seagrasses: Biology, ecology and conservation;. Dordrecht: Springer. 1 vol. (XVI-691). ISBN: 1-4020-2942-X.

Lefebvre A, Thompson C, Amos CL. 2010. Influence of Zostera marina canopies on unidirectional flow, hydraulic roughness and sediment movement. Continental Shelf Research. 30:1783–1794. doi:10.1016/j.csr.2010.08.006.

Luhar M, Nepf HM. 2011. Flow-induced reconfiguration of buoyant and flexible aquatic vegetation. Limnology and Oceanography. 56:2003–2017. en. doi:10.4319/lo.2011.56.6.2003.

Naudascher E, Rockwell D. 1994. Flow-induced Vibrations: IAHR Hydraulic Structures Design Manuals 7. 1st ed. Rotterdam: CRC Press. 432 p. (IAHR Design Manual; v.7). ISBN: 9781351447867.

Okamoto T, Nezu I, Sanjou M. 2016. Flow–vegetation interactions: length-scale of the "monami" phenomenon. Journal of Hydraulic Research. 54:251–262. doi:10.1080/00221686.2016.1146803.

Ondiviela B, Losada IJ, Lara JL, Maza M, Galván C, Bouma TJ, van Belzen J. 2014. The role of seagrasses in coastal protection in a changing climate. Coastal Engineering. 87:158–168. doi:10.1016/j.coastaleng.2013.11.005.

Ozgoren M. 2006. Flow structure in the downstream of square and circular cylinders. Flow Measurement and Instrumentation. 17:225–235. doi:10.1016/j.flow-measinst.2005.11.005.

Park CW, Lee SJ. 2004. Effects of free-end corner shape on flow structure around a finite cylinder. Journal of Fluids and Structures. 19:141–158. doi:10.1016/j.jfluidstructs.2003.12.001.

Pattenden RJ, Turnock SR, Zhang X. 2005. Measurements of the flow over a low-aspect-ratio cylinder mounted on a ground plane. Exp Fluids. 39:10–21. En;en. doi:10.1007/s00348-005-0949-9.

Patterson MR, Harwell MC, Orth LM, Orth RJ. 2001. Biomechanical properties of the reproductive shoots of eelgrass. Aquatic Botany. 69:27–40. doi:10.1016/S0304-3770(00)00133-9.

Paul M, Bouma TJ, Amos CL. 2012. Wave attenuation by submerged vegetation: combining the effect of organism traits and tidal current. Mar. Ecol. Prog. Ser. 444:31–41. doi:10.3354/meps09489.

Paul M, Henry P-YT. 2014. Evaluation of the use of surrogate Laminaria digitata in eco-hydraulic laboratory experiments. J Hydrodyn. 26:374–383. En;en. doi:10.1016/S1001-6058(14)60042-1.

Paul M, los Santos CB de. 2019. Variation in flexural, morphological, and biochemical leaf properties of eelgrass (Zostera marina) along the European Atlantic climate regions. Mar Biol. 166. doi:10.1007/s00227-019-3577-2.

Roshko A. 1954. On the drag and shedding frequency of two-dimensional bluff bodies. National Advisory Committee for Aeronautics. NACA TN 3169.

Schendel A, Hildebrandt A, Goseberg N, Schlurmann T. 2018. Processes and evolution of scour around a monopile induced by tidal currents. Coastal Engineering. 139:65–84. doi:10.1016/j.coastaleng.2018.05.004.

Spalding MD, McIvor AL, Beck MW, Koch EW, Möller I, Reed DJ, Rubinoff P, Spencer T, Tolhurst TJ, Wamsley TV, et al. 2014. Coastal Ecosystems: A Critical Element of Risk Reduction. Conservation Letters. 7:293–301. en. doi:10.1111/conl.12074.

Sumer BM, Fredsøe J. 2006. Hydrodynamics around cylindrical strucures. Rev. ed. Singapore, Hackensack, NJ: World Scientific Pub. 530 p. (Advanced series on ocean engineering; v. 26). ISBN: 9789812700391. eng.

Sumner D. 2013. Flow above the free end of a surface-mounted finite-height circular cylinder: A review. Journal of Fluids and Structures. 43:41–63. doi:10.1016/j.jfluidstructs.2013.08.007.

Vettori D, Nikora V. 2018. Flow–seaweed interactions: a laboratory study using blade models. Environ Fluid Mech. 18:611–636. doi:10.1007/s10652-017-9556-6.

Vlachos PP, Telionis DP. 2008. The Effect of Free Surface on the Vortex Shedding From Inclined Circular Cylinders. J. Fluids Eng. 130. doi:10.1115/1.2829578.

Weiss J. 2019. A Tutorial on the Proper Orthogonal Decomposition. In: AIAA Aviation 2019 Forum. Dallas, Texas: American Institute of Aeronautics and Astronautics. en.